The Astrophysical Journal Supplement Series, 163:270–281, 2006 April

ON THE LENGTHS, COLORS, AND AGES OF 18 FACE-ON BARS

D. A. Gadotti[1,2,3] and R. E. de Souza[1]

Received 2004 October 1; accepted 2005 November 22

ABSTRACT

Along with a brief analysis we present data obtained from *BVRI* and K_s images of a sample of 19 galaxies (18 barred and 1 unbarred), which will be further explored in a future paper. We measured the lengths and colors of the bars, created color maps, and estimated global color gradients. Applying a method developed in a companion paper, we could distinguish for seven galaxies in our sample those whose bars have been recently formed from the ones with already evolved bars. We estimated an average difference in the optical colors between young and evolved bars that may be translated to an age difference of the order of 10 Gyr, meaning that bars may be, at least in some cases, long-standing structures. Moreover, our results show that, on average, evolved bars are longer than young bars. This seems to indicate that, during its evolution, a bar grows longer by capturing stars from the disk, in agreement with recent numerical and analytical results. Although the statistical significance of these results is low, and further studies are needed to confirm them, we discuss the implications from our results on the possibility of bars being a recurrent phenomenon. We also present isophotal contours for all our images as well as radial profiles of relevant photometric and geometric parameters.

Subject headings: galaxies: bulges — galaxies: evolution — galaxies: formation — galaxies: fundamental parameters — galaxies: photometry — galaxies: structure

Online material: extended figure set

1. INTRODUCTION

The formation and evolution of galaxies remain as a major problem in the 21st century astrophysical sciences. Considering the complexity of this theme it could not be different, even facing the tremendous progress done so far. It involves intricate dynamical processes between several different components of the universe: dark matter, gas, and stars. And the proper understanding of the behavior of these components invokes more physical processes, not all of them quite well understood.

The years that marked the demise of the 20th century were also a period that brought a change of perspective in the way this problem is tackled. Manifest in previous thoughts is the idea that the observed properties of galaxies were mostly set up during violent and fast processes in the early stages of galaxy formation. This is a common characteristic in both the monolithic (Eggen et al. 1962) and hierarchical (Searle & Zinn 1978) scenarios of galaxy formation. Referring to these seminal articles, one sees that among their main differences is the timescale for the collapse of the protogalactic clouds and their physical status during the collapse. Modern work, however, based both on observational and theoretical studies, forces the inclusion of slow processes that take place during a Hubble time of galactic evolution, so as to properly understand the observed properties of galaxies. The bottom line is that, even being slow, but because they happen so extensively in time, secular evolutionary processes are as important as galaxy formation processes to determine what these stellar systems are, as well as how they reached their present physical configuration.

This subject has been recently and beautifully reviewed by Kormendy & Kennicutt (2004). In their thorough analysis of many previous results, based on both observational and theoretical studies, it is concluded that one major consequence of secular evolution is the building of (pseudo) bulges (see also Athanassoula 2005). These are central galactic structures that produce light in excess of that from the exponential disk but are *not* classical bulges (i.e., they are not formed through collapse or mergers). In fact, pseudobulges keep a record on their disk origin via nonaxisymmetric forces induced by internal components, mainly bars, but also by oval disks and triaxial halos, and are generally flat and disklike (whereas classical bulges are supposed to be spheroidal or weakly triaxial). As pointed out by Athanassoula (2005) these different types of bulges can coexist in the same galaxy. The influence of bars in galactic evolution, as Kormendy & Kennicutt (2004) show, has many other facets, including the building of a reservoir to fuel the active nuclei of galaxies.

On the other hand, theories of bar formation and evolution are still in full development, as the problem posed by asking how bars form and evolve has led us to many interesting difficulties (see, e.g., Gadotti & de Souza 2003a and references therein; see also Gadotti & de Souza 2003b). Recently, Athanassoula & Misiriotis (2002) and Athanassoula (2002, 2003) presented promising models in the direction of a more definite answer. These models also introduce a change of paradigm by revealing that dark matter halos, when realistically treated, may lead to bar strengthening rather than inhibit this instability, a belief that was spread by earlier experiments with rigid halos. Another key point introduced by these models refers to the aging of bars. These models show that bars should become longer as they evolve. Observational tests of these models, however, are still lacking (but see Laurikainen et al. 2004).

In a companion paper (Gadotti & de Souza 2005, hereafter Paper I) we introduce a new method that enables us to discriminate between recently formed and evolved bars. Since bars are the main driver of internal secular evolution in disk galaxies and the slow building of their central components, the next logical

[1] Departamento de Astronomia, Universidade de São Paulo, Rua do Matão 1226, 05508-090 São Paulo-SP, Brazil; ronaldo@astro.iag.usp.br.

[2] Laboratoire d'Astrophysique de Marseille, 2 Place Le Verrier, 13248 Marseille Cedex 04, France.

[3] Present Address: Max-Planck-Institut für Astrophysik, Karl-Schwarzschild-Strasse 1, D-85748 Garching bei München, Germany; dimitri@mpa-garching.mpg.de.

TABLE 1
BASIC DATA FOR ALL GALAXIES IN OUR SAMPLE

Name (1)	Type (2)	D_{25} (3)	log R_{25} (4)	m_B (5)	cz (6)	d (7)	AGN (8)	Companion (9)
IC 0486	SBa	0.93	0.11	14.60	7792	111.3	Sey1	M
NGC 2110	SAB0	1.70	0.13	...	2064	29.5	Sey2	N
NGC 2493	SB0	1.95	0.00	12.91	4060	58.0	...	N
NGC 2911	SA0(s)	4.07	0.11	12.21	3195	45.6	Sey/LINER	Y
NGC 3227	SABa(s)	5.37	0.17	11.59	1235	17.6	Sey1.5	Y
NGC 4151	SABab(rs)	6.31	0.15	10.90	1190	17.0	Sey1.5	M
NGC 4267	SB0(s)	3.24	0.03	11.73	1123	16.0	...	N
NGC 4303	SABbc(rs)	6.46	0.05	10.21	1620	23.1	Sey2	Y
NGC 4314[a]	SBa(rs)	4.17	0.05	11.22	1146	16.4	LINER	N
NGC 4394[a,b]	SBb(r)	3.63	0.05	11.53	1036	14.8	LINER	Y
NGC 4477	SB0(s)	3.80	0.04	11.27	1441	20.6	Sey2	Y
NGC 4579[a]	SABb(rs)	5.89	0.10	10.68	1607	23.0	LINER/Sey1.9	N
NGC 4593	SBb(rs)	3.89	0.13	11.67	2498	35.7	Sey1	M
NGC 4608[a,b]	SB0(r)	3.24	0.08	11.96	1893	27.0	...	N
NGC 4665	SB0/a(s)	3.80	0.08	11.50	872	12.5	...	N
NGC 5383[a,b]	SBb(rs)	3.16	0.07	12.18	2472	35.3	...	Y
NGC 5701[a,b]	SB0/a(rs)	4.26	0.02	11.82	1601	22.9	LINER	N
NGC 5850[a,b]	SBb(r)	4.26	0.06	12.04	2637	37.7	...	N
NGC 5936[b]	SBb(rs)	1.44	0.05	13.01	4147	59.2	...	N

NOTES.—Cols. (1) and (2) show, respectively, the name and the morphological type of the galaxy, while col. (3) shows its diameter in arcmin at the 25 B magnitude isophotal level, and col. (4) shows the decimal logarithm of its major-to-minor axes ratio at the same level. Cols. (5) and (6) show, respectively, the apparent B magnitude and the radial velocity in km s^{-1}. All of these data were taken from the RC3, except the radial velocity, taken from the Lyon Extragalactic Data Archive (hereafter LEDA), corrected for infall of the Local Group toward Virgo. Col. (7) gives the distance to the galaxy in Mpc, using the radial velocity in col. (6) and $H_0 = 70$ km s^{-1} Mpc^{-1}. Col. (8) presents an AGN classification according to NED. In col. (9), "Y" means that there is a companion galaxy similar in size physically interacting within 10′, while "N" means that there are no companion galaxies; "M" indicates that there are companion galaxies that lack redshift data and thus may be only projection effects. To make this analysis we used the RC3 and LEDA.

[a] Indicates those galaxies in common with Paper I that also have bar age estimates.

[b] Indicates those galaxies with images also in the near-infrared.

step is evidently to explore links between the ages of bars and the global physical properties of galaxies. In this paper, we proceed along this course with the help of multiband optical and near-infrared CCD images of a sample of 19 galaxies, of which 7 have bar age estimates. In the next section we describe the sample and the acquisition and treatment of the images. Section 3 is devoted to explaining how we have obtained the relevant physical parameters for the discussion we address further on—that is, how we estimated bar lengths and, from the color information in the multiband images, global color gradients in our sample galaxies and the color of their bars. In § 4 we explore these data, and finally, in § 5, we address a general discussion and the implications from our results on the current knowledge concerning bar formation and secular evolution. The data presented in this paper will be used in a future paper, where we will apply a multicomponent image decomposition code to explore possible relationships between the structural properties of bulges, disks, and bars. We used a value for the Hubble constant of $H_0 = 70$ km s^{-1} Mpc^{-1}.

2. DATA ACQUISITION

This section describes the main properties of our sample galaxies as well as details in the acquisition and treatment of the optical and near-infrared CCD images. For the sake of clarity this is done in separate subsections.

2.1. *The Sample*

The more relevant properties of the 19 galaxies of our sample are displayed in Table 1. All of them were observed in B, V, R, and I, except NGC 4593, for which we could not acquire B images. For six of them we also obtained images in the near-infrared K_s broad band. One may easily verify that this sample has general characteristics similar to that in Paper I; indeed, both samples have seven galaxies in common, and for those we also have bar age estimates. We have not looked for a complete, unbiased sample, but instead we chose interesting galaxies that could shed some light on the subjects we are discussing. While all galaxies are local, bright, and close to face-on, they span a range in morphologies. According to de Vaucouleurs et al. (1991, hereafter RC3), there is 1 SA (unbarred) galaxy, 5 SAB (weakly barred) galaxies, and 13 SB (strongly barred) galaxies. Eight galaxies have morphological types S0 or S0/a, 4 are Sa or Sab, and the remaining 7 go as late-type as Sbc. Table 1 also shows that in our sample there is a significant fraction of galaxies that have nuclei with nonstellar activity and/or an identified companion that may be gravitationally interacting.

This variety might be helpful in trying to evaluate clues related, for instance, to the prominence of the bulge, the bar length, and the gravitational perturbation of a companion. The presence of galaxies with active nuclei will also be relevant to help in understanding the role played by bars in the fueling of this phenomenon.

The choice for bright and face-on galaxies assures us more reliable estimates for the structural parameters of these galaxies, since it means higher signal-to-noise ratio (S/N) and spatial resolution, and since in more edge-on systems a proper description of, e.g., the bar may be unattainable. Face-on systems also ease the interpretation of colors and color gradients as the effects of dust are minimized.

2.2. *Acquisition and Treatment of the Optical Images*

The optical imaging was done in the B, V, R, and I broad bands in 1999 February and May, and in 2000 February and March, in a total of 9 observing nights. It was performed at the Kuiper 1.55 m

TABLE 2
SUMMARY OF THE OPTICAL OBSERVATIONS AND CALIBRATIONS

Night	Galaxy	Seeing (arcsec)	Photometric?	Error (*B*)	Error (*V*)	Error (*R*)	Error (*I*)
1999 Feb 17	N2493	1.4	No				
1999 May 9	N4680; N5701; N5936BVR	1.4	Yes	0.01	0.01	0.01	0.01
1999 May 10	N4267; N4665; N5850	1.3	No				
1999 May 11	N4394; N4477; N5936I	1.2	Yes	0.04	0.02	0.01	0.35
1999 May 12	N4314; N5383	1.2	Yes	0.05	0.01	0.02	0.38
2000 Feb 1	I0486; N3227; N4593VRI	1.4	Yes				
2000 Feb 2	N2110	1.5	Yes	0.01	0.02	0.01	0.02
2000 Feb 3	N2911; N4151; N4579	1.4	No				
2000 Mar 3	N4303	1.3	Yes	0.01	0.01	0.01	0.01

NOTES.—Galaxies observed in each usable night of the observing runs. When no band is specified the observations were done in *B*, *V*, *R*, and *I*. The average seeing in the *R* band in arcsec and the photometric conditions are also displayed, along with the photometric zero-point error from standard calibration in each band. In the nights when no standard stars were observed, the zero point of the closest photometric night was applied.

telescope operated by the University of Arizona Steward Observatory on Mount Bigelow. We used its Cassegrain f/13.5 focus and the back-illuminated CCD No. 24, with a gain of 3.5 e^- ADU^{-1} and a readout noise of 8.7 e^-. This CCD has 2048×2048 21 μm pixels, but we used it binned in 2 per 2 pixels. Thus, the plate scale of these observations is 0.″29 pixel^{-1}, and their field of view is roughly about 5′ on a side. The filter transmission curves are similar to the Johnson-Morgan system for *B* and *V*, and to the Cousins system for *R* and *I* (see, e.g., Fukugita et al. 1995; Kitchin 1998). Table 2 shows a summary night log with relevant information.

To ease cosmic ray removal, we have taken several exposures for each galaxy. These were 5 in *B* and *V*, and 3 in *R* and *I* with an integration time of 300 s each. Standard stars from Landolt (1983) were used for photometric calibration. This was done in the standard manner within the IRAF[4] environment. Table 2 also shows a summary of these calibrations. To correct extinction caused by the atmosphere, appropriate coefficients were determined for each band. Note that the photometric errors are larger in the *I* band, which is expected as this band covers sky emission lines and its images had to be corrected from fringing effects.

Preprocessing of the images for analysis was also performed with IRAF. Bias images were subtracted from all science images and the latter were normalized with dome flat fields in the usual manner. Fringes in the *I* band images were removed with the `mkfringecor` task. Finally, bad pixels were also eliminated but the detectors used were cosmetically clean.

To eliminate cosmic rays and raise the final S/N in the science images, we used the `imcombine` task to combine by the median multiple exposures of each galaxy in each band. Small shifts between the exposures were calculated with the `imcentroid` task and 3–5 reference stars.

To remove the contribution from the sky, we first edited the combined images, removing the galaxy and foreground stars. This was done using the task `imedit` with a circular aperture and replacing the selected pixels by background pixels with a Gaussian noise distribution added. After that, we determined the mean sky background and its standard deviation. Then we removed all pixels whose values were discrepant from the mean background by more than 3 times the standard deviation. A sky model was obtained by fitting with `imsurfit` a linear surface to the image, and this model was subtracted from the combined image. Finally, we removed objects such as foreground stars and bright H II regions from the sky-subtracted image to get a final science image for each galaxy in *B*, *V*, *R*, and *I*. It should be noted, however, that for four galaxies (NGC 3227, NGC 4151, NGC 4303, and NGC 4579) our images may not contain areas in which there is only a background contribution. This means that the sky contribution may have been overestimated. Hence, the faintest parts of their optical surface brightness profiles may be subject to this source of error.

[4] IRAF is distributed by the National Optical Astronomy Observatory, which is operated by the Association of Universities for Research in Astronomy, Inc., under cooperative agreement with the National Science Foundation.

2.3. *Acquisition and Treatment of the Near-infrared Images*

Images in the near-infrared K_s band were acquired for six galaxies in our sample with the 2.29 m Bok telescope operated by the University of Arizona Steward Observatory on Kitt Peak. Observations occurred in 5 nights during 1999 May and June. The focal ratio in the Cassegrain mode was f/45. We used a Rockwell infrared detector with 256^2 pixels, with a readout noise of 30 e^- and gain of 15 e^- ADU^{-1}. The pixel size on sky was 0.″59, and the field of view nearly 2.′5. The filter's transmission curve is approximately flat from 2.0 to 2.3 μm with sharp cutoffs. Table 3 shows relevant data on the near-infrared observations and photometric calibrations.

Our observing strategy in the K_s images was typically to obtain two exposures of 30 s in the galaxy, followed by two sky exposures of 30 s in regions relatively free of objects a few arcmin away from the galaxy, which serve for sky subtraction. Such a cycle is repeated several times in a square dither pattern with shifts of several arcsec. These procedures avoid space and time sky changes and the effects of bad pixels; also, as the field of view is restricted, it allows us to cover a larger area of the galaxy than with just one pointing. In those galaxies with an angular apparent diameter larger than our images, the loss is restricted to the disk outskirts and does not compromise our analysis. In particular, the bar is always entirely visible.

For the photometric calibration we observed standard stars from Elias et al. (1982) and Persson et al. (1998) and determined an atmospheric extinction correction coefficient. As this calibration in the near-infrared is prone to more errors than in the optical case, we observed many standard stars and most of them at several zenithal distances. Table 3 displays the photometric errors calculated in the nights they were observed.

In the treatment of the near-infrared images we used the GEMINI IRAF package. Flat-field images were obtained through the `qflat` task from all sky images related to a determined galaxy. The QSKY task was used to estimate the sky contribution from each cycle. These corrections were performed by `qreduce`.

TABLE 3
SUMMARY OF THE NEAR-INFRARED OBSERVATIONS AND CALIBRATIONS

Night	Galaxy	Seeing (arcsec)	Photometric?	Error (K_s)	t (s)
1999 May 4.....	N4608; N5850	1.2	Yes	0.03	570; 900
1999 May 5.....	N5701	1.3	Yes	0.09	1350
1999 May 29.....	N5936	1.2	No		180
1999 May 31.....	N5383	1.1	Yes	0.03	840
1999 Jun 1	N4394	1.2	Yes		230

NOTES.—Galaxies observed in each usable night of the observing runs. The average seeing in arcsec and the photometric conditions and errors after standard calibration are also displayed. The total exposure time for each galaxy is in seconds in the last column. In the nights when no standard stars were observed, the zero point of the closest photometric night was applied.

Finally, the `imcoadd` task combines by the median all corrected images of a galaxy calculating the necessary shifts due to the dither pattern and also corrects bad pixels.

3. OBTAINING RELEVANT PHYSICAL PARAMETERS

3.1. *Bar Lengths*

Using our images and the `ellipse` task in IRAF we built for each galaxy in each band radial profiles of the elliptically averaged surface brightness, as well as geometric parameters of the isophotes, namely, position angle, ellipticity, and the b4 Fourier coefficient. The results are shown in Figure Set 1, which also displays our images and isophotal contours. During the ellipse fitting the center was held fixed. To find the galaxy center, we first run `ellipse` with the center free and choose the center as the average of the values chosen by the task at a radius around 10–15 pixels. The radius for each fit grows logarithmically at a 10% rate.

The optical surface brightness profiles were corrected from the extinction by the Galaxy following the maps of Schlegel et al. (1998) in the NASA Extragalactic Database (NED). For the sake of precision, we applied a first order correction for the dust extinction caused within the galaxies themselves; we used the results from Giovanelli et al. (1994) that find a relation between the galaxy inclination and the extinction, which may be expressed in I magnitudes as

$$A_I = 1.12(\pm 0.05) \log R_{25}. \quad (1)$$

To find the analogous equations for the other optical bands, one just needs to apply the results of Elmegreen (1998), which show that the extinction in B, V, and R is, respectively, 3.17, 2.38, and 1.52 times larger than in I.

We next tried to estimate the lengths of the bars, L_B, in the galaxies of our sample in as reliable a fashion as possible. This was done by calculating the average radius where the end of the bar is detected in the V and R images through three different criteria: a peak in the ellipticity radial profile, the mean point of an abrupt change in position angle (in the cases where the position angle of the bar is different from that of the disk), and the point at which the galaxy surface brightness profile drops to join back the light distribution in the disk—in the bar region there is of course an excess of light if one compares it to the profile of an unbarred galaxy or the exponential profile of the disk (see Fig. Set 1). We also noticed that near the end of the bar, but somewhat closer to the center, there is a peak in the b4 Fourier component, which is expected due to the nonaxisymmetric nature of the bar. We used only the V and R images in this analysis aiming to obtain a compromise between S/N and a better representation of the majority of the stellar population in the galaxies, but we did verify that no discrepancies would arise if other band images were used instead.

Since most of our galaxies are close to face-on, projection effects on the bar length estimates are negligible. However, five barred galaxies in our sample may be somewhat inclined systems as their log R_{25} parameter is larger than 0.1 (and assuming that their outermost isophotes are intrinsically circular; see Table 1). Their projected (observed and measured) bar lengths thus may be, in principle, underestimated if compared to the real lengths. Fortunately, however, in each of these galaxies the position angle of the bar is very similar to that of the line of nodes (the largest misalignment is $\sim 20^\circ$), meaning that the bar length would not change significantly after deprojecting the galaxy image. We made this analysis using our data as well as that present in LEDA and in NED and found an excellent agreement. Obtaining deprojected measurements for the bar lengths could also introduce errors from the uncertainties in the inclination angle and the position angle of the line of nodes. To consider that the outermost isophotes of disk galaxies are intrinsically circular may not be a safe assumption. In addition, deprojection techniques assume that the whole galaxy is flat, which is not the case of evolved, vertically thickened bars. We believe that taking projection effects into account would only prove useful (rather than harmful) if most of the galaxies in our sample were far from face-on and if our sample was sufficiently large to significantly put down statistical random errors in the measurements of L_B itself. A discussion on the advantages and disadvantages of deprojecting galaxy images can also be found in Jungwiert et al. (1997) and in Erwin & Sparke (2003). Furthermore, since none of these more inclined galaxies in our sample were studied in Paper I, and then had the age of their bars evaluated, the main results of this paper would remain unchanged even after considering projection effects.

We looked for a correlation between L_B and D_{25} from our B images (and from the RC3 when necessary, i.e., for NGC 4303, NGC 4593, and NGC 5850; in the remaining cases our values agree well with those from RC3), and a trend was found but with a large spread (the linear correlation coefficient is 0.5, see Fig. 2). This means that it is not necessarily true that bigger galaxies have bigger bars, anticipating that L_B might also be ruled by another physical process(es). Table 4 shows the results. It is interesting to note, however, that Laine et al. (2002) found a somewhat better correlation (their linear correlation coefficient is 0.66). Recently, Erwin (2005) also found a better correlation. Nonetheless, his results show that the correlation is stronger for S0 galaxies and weakens significantly toward later morphological types. In fact, he found that bars in S0–Sab galaxies extend to $\sim(0.2–0.8)R_{25}$, whereas late-type bars extend to only $\sim(0.05–0.35)R_{25}$. These figures also reflect the significant fluctuations in the correlation.

Measuring bar lengths has ever proved a harder task than it seems. Thus, a comparison of our results to those already published might be useful. For eight galaxies of our sample a method

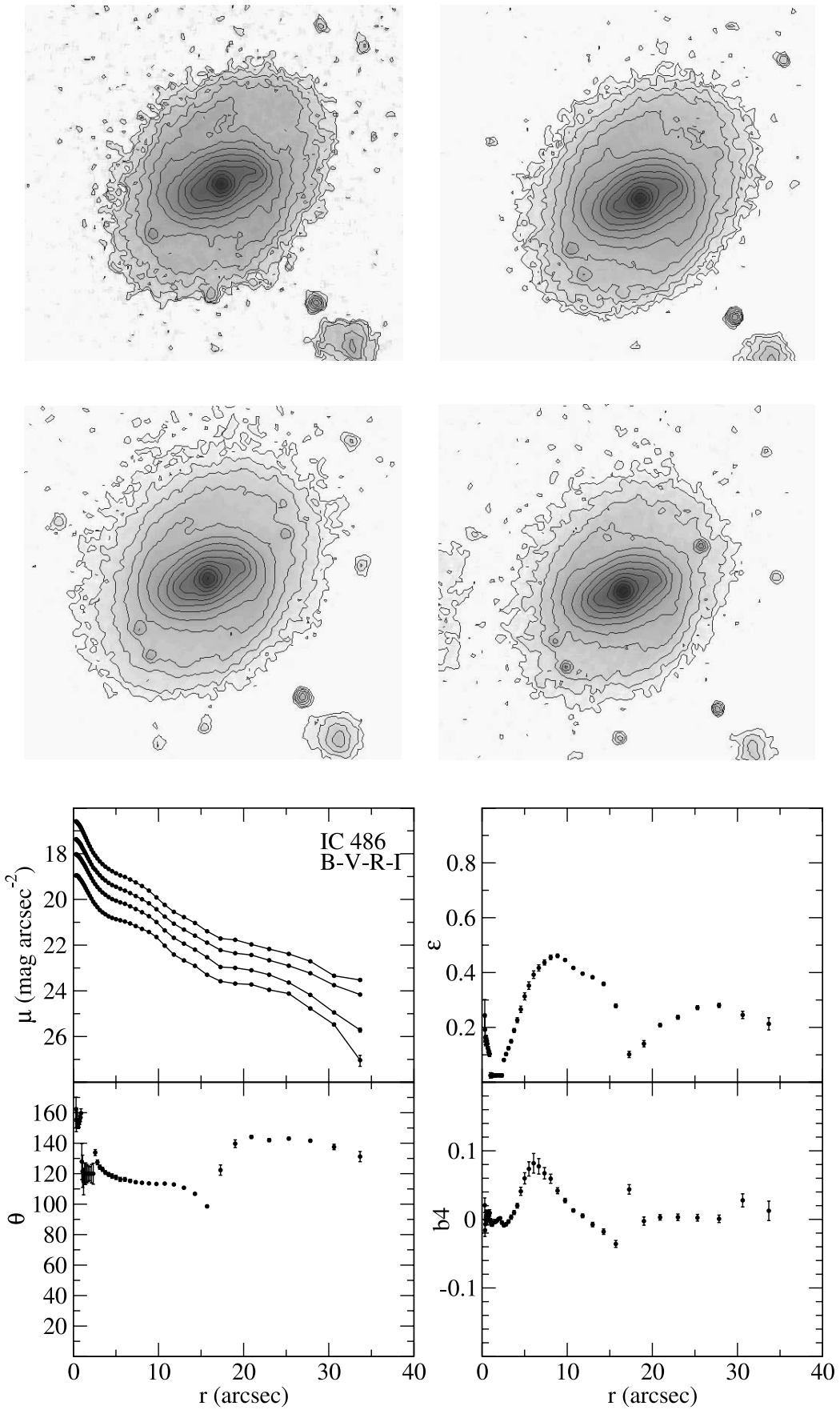

FIG. SET 1.—Results of the ellipse fitting to the optical and near-infrared images of all galaxies in our sample. Each CCD image is median-filtered and has isophotal contours overlaid, spaced by 0.5 mag arcsec^{-2}. In the optical bands the images refer to *B*, *V*, *R*, and *I* broad bands from top to bottom. The radial profiles are of surface brightness (*top left*), position angle (*bottom left*), ellipticity (*top right*), and the b4 Fourier coefficient (*bottom right*). Position angles grow from north at 0° through east at 90°. North is up, and east is to the left in all optical images. In the near-infrared images north is up, and east is to the right. [*See the electronic edition of the Supplement for Figs. 1.2–1.25*]

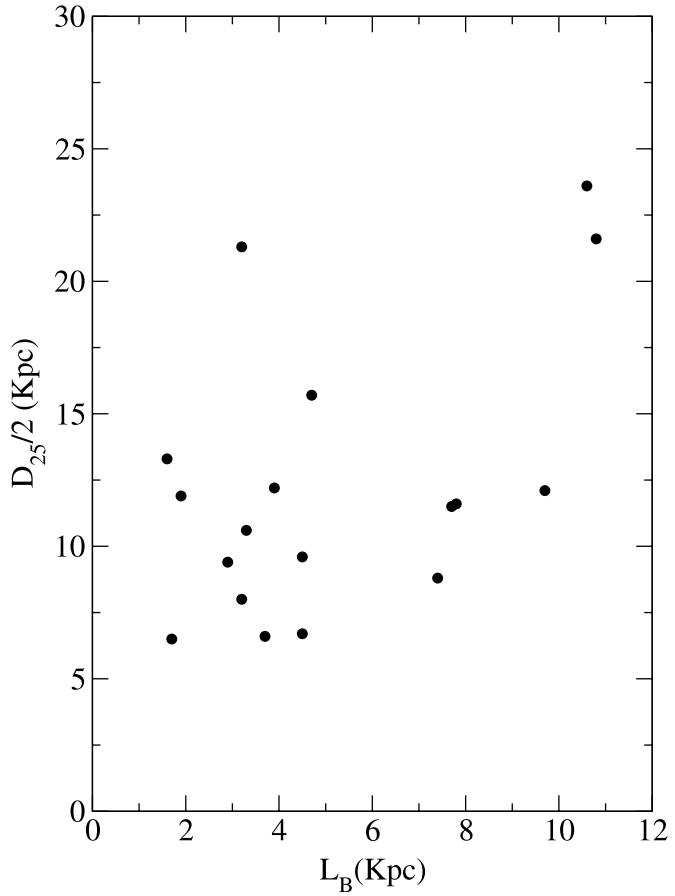

FIG. 2.—Radius of the 25 B mag arcsec^{-2} isophote plotted against the length of the bar, i.e., its semimajor axis.

was already applied to estimate the bar length, and in some cases more than one method. Martin (1995) made visual measurements of L_B on photographic plates of good linear scale for three of these galaxies: NGC 4303, where his estimates point to a value of 2.2 kpc, whereas ours give 3.2 kpc; NGC 4394, again with estimates shorter than ours, 2.5 kpc against 3.7 kpc; and NGC 5850, where, remarkably, our estimates are identical, 10.6 kpc. In the next studies we will discuss, bar lengths were also measured through the analysis of geometrical properties of the isophotes but the choice for radius is different. Wozniak et al. (1995) chose the bar radius as the one where the ellipticity drops to a local minimum after the maximum reached in the bar. They measured L_B for NGC 4593 as 10.4 kpc, whereas we found 10.8 kpc. They also give L_B for NGC 5850: 14.8 kpc, considerably in excess of the values above. The bar in the latter has also been measured by Erwin (2004), who arrived to the intermediate value of 13.7 kpc. His choice for the bar radius is the minimum between the radius of the local minimum in ellipticity (as in Wozniak et al. 1995) and the radius, after the ellipticity peak in the bar, where the position angle changes by at least 10°. He also presents estimates for L_B in NGC 4303 (3.8 kpc, whereas ours is 3.2 kpc) and NGC 4314 (6.3 kpc, while ours is 7.4 kpc). Using similar criteria, Erwin & Sparke (2002, 2003) give L_B for NGC 4665 as 2.7 kpc, while we found 3.2 kpc. Finally, Jungwiert et al. (1997) discuss bar lengths as the point at which the ellipticity peaks, finding for NGC 4267 an L_B of 1.5 kpc (we found 1.7 kpc) and for NGC 5701 an L_B of 4.2 kpc (while our result is 4.5 kpc). The mean difference between our estimates and those in the literature is about 19%. Altogether, one sees general agreement, but the discrepancies mean that the task of finding a better definition for the bar length is certainly one worthy to pursue.

3.2. *Bar Colors and Galaxy Global Color Gradients*

In Figure 3 we display optical color profiles for the galaxies in our sample, whereas Figure 4 presents $B - R$ color maps (except for NGC 4593, where the color map refers to $V - R$). The color profiles were built from the ellipse fits. Although the set of ellipses

TABLE 4
GLOBAL COLOR GRADIENTS AND BAR COLOR AND LENGTH

Galaxy	$G(B-V)$	$G(B-R)$	$G(B-I)$	$(B-I)_B$	L_B (kpc)	$2L_B/D_{25}$
I486	−0.17 ± 0.01	−0.17 ± 0.01	−0.34 ± 0.01	1.44	4.7	0.30
N2110	−0.08 ± 0.01	−0.13 ± 0.01	−0.11 ± 0.01	1.46	3.3	0.31
N2493	−0.19 ± 0.01	−0.18 ± 0.01	−0.21 ± 0.01	2.44	7.7	0.67
N2911	−0.09 ± 0.01	−0.21 ± 0.01	−0.36 ± 0.01	...	...	...
N3227	0.11 ± 0.01	−0.16 ± 0.02	−0.09 ± 0.02	1.71	1.9	0.16
N4151	0.25 ± 0.01	0.31 ± 0.02	0.63 ± 0.03	1.62	4.5	0.67
N4267	0.04 ± 0.00	0.08 ± 0.00	0.10 ± 0.01	2.48	1.7	0.26
N4303	−0.25 ± 0.04	−0.26 ± 0.03	−0.29 ± 0.04	1.08	3.2	0.15
N4314	0.02 ± 0.01	−0.08 ± 0.02	−0.05 ± 0.02	1.90	7.4	0.84
N4394	−0.09 ± 0.01	−0.17 ± 0.01	−0.17 ± 0.02	1.30	3.7	0.56
N4477	−0.09 ± 0.01	−0.14 ± 0.02	−0.17 ± 0.02	1.60	2.9	0.31
N4579	−0.11 ± 0.01	−0.14 ± 0.01	−0.13 ± 0.01	1.89	3.9	0.32
N4608	−0.07 ± 0.01	−0.02 ± 0.01	−0.15 ± 0.01	2.05	7.8	0.67
N4665	−0.10 ± 0.01	−0.23 ± 0.01	−0.03 ± 0.02	2.18	3.2	0.40
N5383	−0.43 ± 0.04	−0.50 ± 0.05	−0.57 ± 0.07	1.29	9.7	0.80
N5701	0.02 ± 0.00	−0.07 ± 0.01	−0.10 ± 0.01	2.32	4.5	0.47
N5850	−0.12 ± 0.01	−0.14 ± 0.01	−0.09 ± 0.01	2.40	10.6	0.45
N5936	−0.38 ± 0.02	−0.48 ± 0.03	−1.14 ± 0.04	1.34	1.6	0.12
Galaxy		$G(V-R)$	$G(V-I)$	$(V-I)_B$	L_B	$2L_B/D_{25}$
N4593		−0.13 ± 0.01	−0.01 ± 0.01	0.92	10.8	0.50

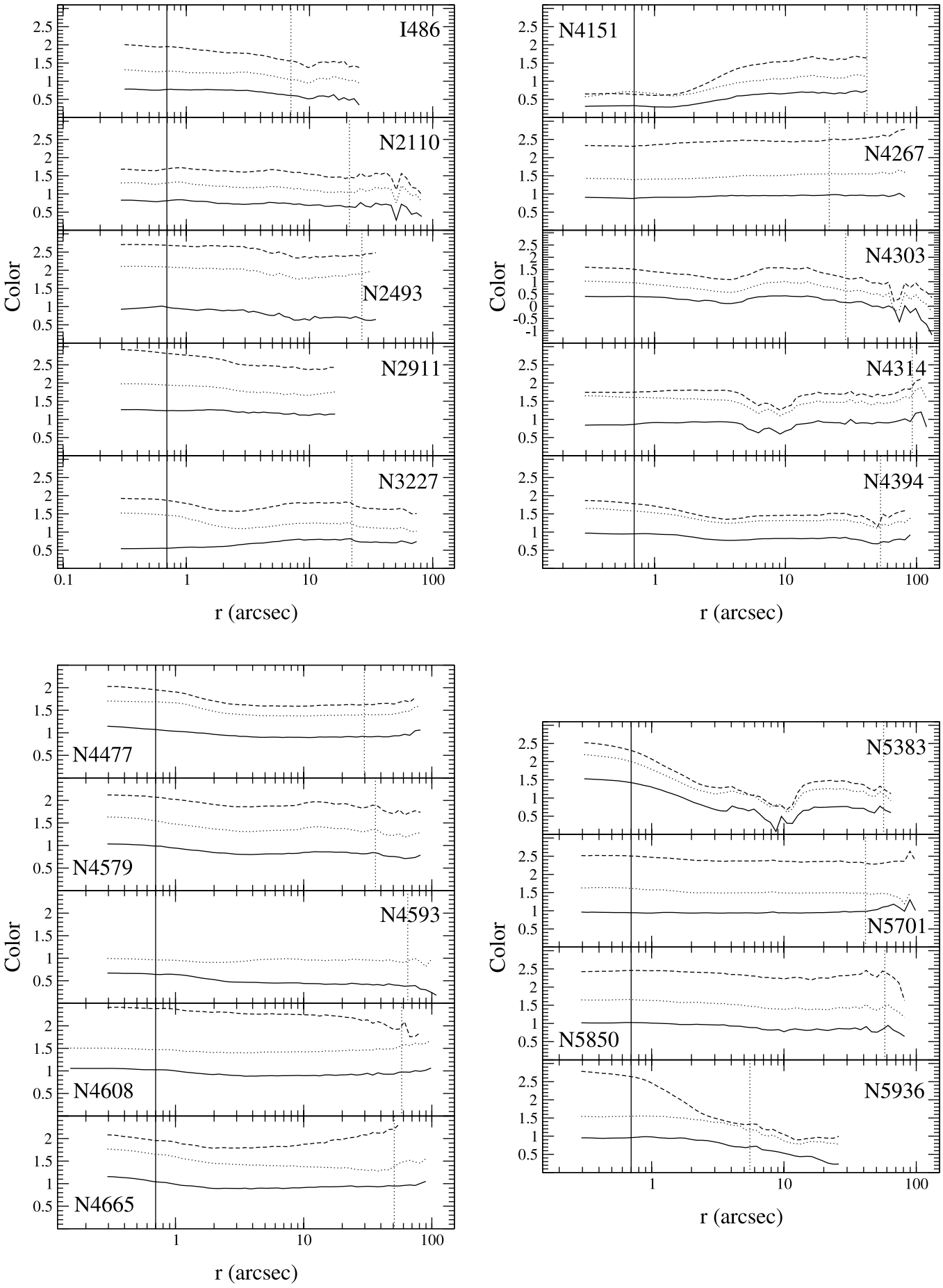

FIG. 3.—Color profiles for all galaxies in our sample. The solid line refers to $B - V$, the dotted line to $B - R$, and the dashed line to $B - I$. The vertical solid line indicates the typical seeing, while the dotted line is our estimate for L_B, from which the color of the bar is derived. Color units are magnitudes, and the ordinate is the galactocentric radius expressed in units of arcsec in a logarithmic scale.

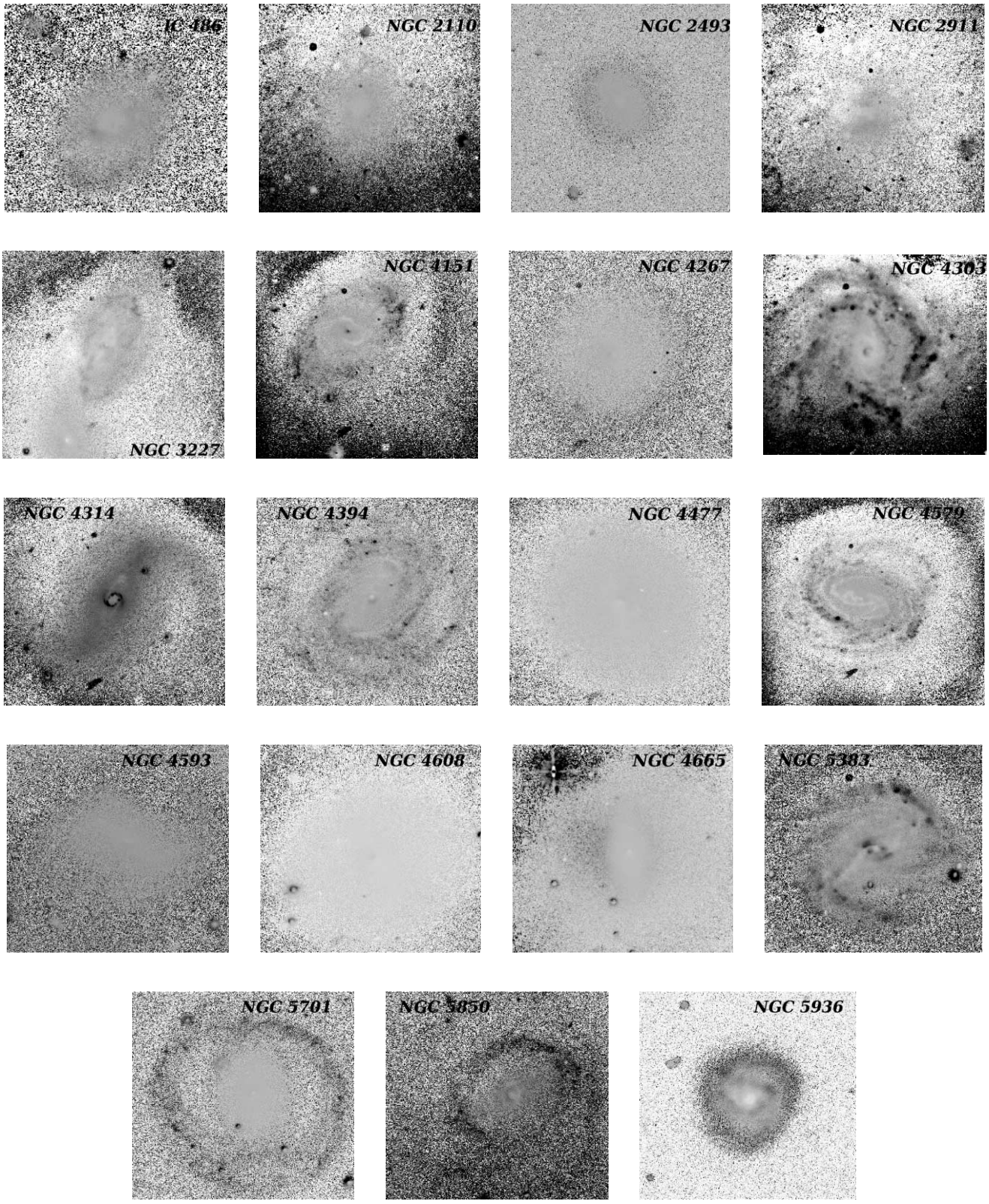

FIG. 4.—$B - R$ color maps for the galaxies in our sample, except for NGC 4593, where it is $V - R$. Darker areas indicate bluer colors.

used are not exactly the same in each band, the relevant geometrical properties of the ellipses are generally identical in different bands, and thus light from different parts of the galaxy in different bands is not mixed. From the color profiles we have estimated $B - V$, $B - R$, and $B - I$ color gradients for all galaxies, except for NGC 4593, whose color gradients refer to $V - R$ and $V - I$. The gradients were calculated through linear regression and the least-squares method, excluding the nuclear region affected by seeing. Moreover, we have also eliminated outlier points by visual inspection to avoid spurious results, but this scarcely happened. Thus, these color gradients represent a global galaxy tendency. The gradients are expressed as in Gadotti &

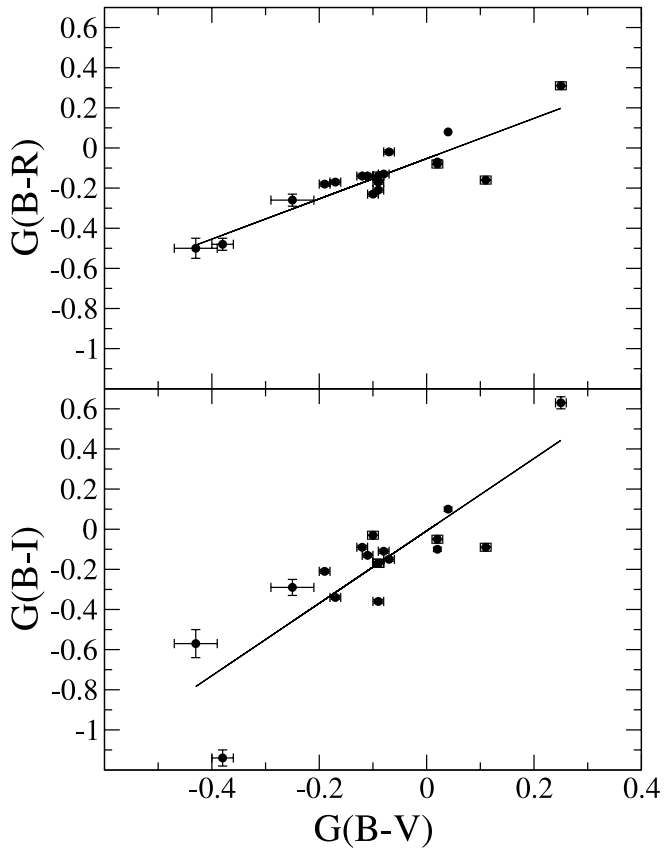

FIG. 5.—$G(B-R)$ and $G(B-I)$ plotted against $G(B-V)$. The solid lines are linear fits to the data in each panel.

dos Anjos (2001), i.e., $G(X-Y) \equiv \Delta(X-Y)/\Delta \log A$, where $X-Y$ is the color index and A is the isophote diameter in units of 0.′1. Using these profiles we also estimated the $B-I$ color of the bars, $(B-I)_B$. These were obtained at the point that marks the end of the bar, i.e., L_B, but we have also avoided star-forming sites that could lead to misleading results. The choice for the $B-I$ index is discussed below. All of these parameters are shown in Table 4. These color values are all corrected for dust reddening in the Galaxy, and inclination corrections were also applied (again, for the sake of precision). We used the same correction as for the surface brightness, except, of course, that we now used the color excess $E(X-Y) = A_X - A_Y$.

The correlations between the different color gradients are shown in Figure 5. As was already discussed in other studies (e.g., de Jong 1996; Gadotti & dos Anjos 2001), these correlations show that the same physical process is responsible for creating these gradients. These color gradients could be a result of either metallicity, age, or dust effects, but Gadotti & dos Anjos (2001) argue that, at least for late-type spirals (around type Sbc), it is the age of the stellar population that is mostly responsible for the global color gradients. From the plots one may linearly fit

$$G(B-R) = -0.05(\pm 0.02) + 1.00(\pm 0.12) \times G(B-V), \quad (2)$$

and

$$G(B-I) = -0.01(\pm 0.05) + 1.80(\pm 0.27) \times G(B-V), \quad (3)$$

which means that $G(B-V)$ and $G(B-R)$ are almost equivalent and suggests that $G(B-I)$ may be more sensitive to variations in the stellar population ages, since the slope in equation (3) is steeper. Note, however, that the scatter in the $G(B-I)/G(B-V)$ relation is also larger; but since the overall trend is similar in both plots of Figure 5 the results concerning bar colors should in principle not depend significantly on the choice of color index.

4. ANALYSIS

4.1. *Does Bar Color Give Bar Age?*

From Table 4 one can see that the mean value for the bar color index $(B-I)_B$ is 1.79 ± 0.11.[5] In Paper I we show that judging from the kinematical analysis NGC 4314, NGC 4608, NGC 5701, and NGC 5850 have evolved bars, whereas those in NGC 4394, NGC 4579, and NGC 5383 are recently formed. The average $(B-I)_B$ of the former is 2.17 ± 0.12, while that of the latter is 1.49 ± 0.20. Old bars are on average 0.68 mag redder than young ones, and this difference is significant at the 3 σ confidence level.[6] Obviously, the color of the bars reflect not their ages but the ages of their stars. However, barred galaxies follow two different patterns regarding star formation (Phillips 1993, 1996; Martin & Friedli 1997). Later type spirals show star-forming sites *along* their bars that are shorter and have an exponential luminosity profile (Elmegreen & Elmegreen 1985). Earlier type spirals, with longer bars that have flat luminosity profiles, lack any star formation along their bars but present star-forming sites in their nuclear and inner rings. Martin & Roy (1995) and Friedli & Benz (1995) argue that star formation along the bars could indicate that these structures are young ($\lesssim$1 Gyr). Thus, the age of the stellar population within the bar may be an indication of the age of the bar itself. It is also suggested by our results that the evolved bars from Paper I indeed have redder colors than the recently formed bars. Nevertheless, we are neglecting effects from differential dust extinction along the bar and the age-metallicity degeneracy, but this seems to be fairly justified since $(B-I)_B$ is measured very far from the centers of the galaxies (where dust extinction is more pronounced), and considering the results from Gadotti & dos Anjos (2001; see also de Jong 1996) that global color gradients are not affected by dust and are mainly sensible to the age, rather than to the metallicity, of the stellar population. In addition, since the galaxies in our sample are in general close to face-on, dust extinction is further minimized.

The average $B-V$ color of the bars that the results from Paper I indicate as evolved bars is 1.1, whereas that of the young bars is 0.7. Theoretical studies of the evolution of the stellar population in galaxies (e.g., Tinsley & Gunn 1976; Maraston 1998) indicate that the mean age of the stars in the latter case is about 1–2 Gyr, while the mean age of the stellar population in evolved bars would be at the order of 15–20 Gyr. Although these results are model dependent, a reasonable difference in age from young and evolved bars seems to be of the order of 10 Gyr. This result reinforces those by Shen & Sellwood (2004) that indicate that bars are a robust structure (see also Elmegreen et al. 2004; Jogee et al. 2004), and also our results from Paper I, in which we suggest a slow mechanism for the vertical evolution of bars, namely, the Spitzer-Schwarzchild mechanism (Spitzer & Schwarzschild 1951, 1953).

4.2. *Do Bars Grow Longer while Aging?*

The recent theoretical studies by Athanassoula & Misiriotis (2002) and Athanassoula (2002, 2003) suggest that during its evolution bars grow longer by capturing stars from the disk and

[5] Errors quoted are the standard error on the mean, corresponding to 1 σ confidence level.

[6] Even so, this result should be carefully considered since with the small number of galaxies in this analysis the mean and the errors are poorly determined.

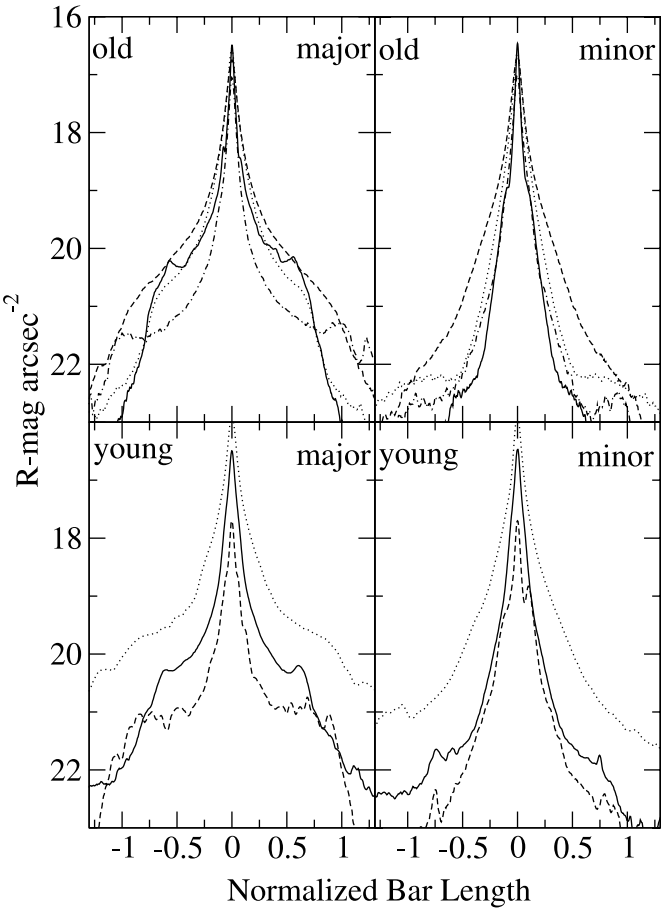

FIG. 6.—*R*-band profiles of the bar major and minor axes for recently formed and evolved bars.

redistributing angular momentum along the disk and halo. In Paper I we show that, while NGC 4314, NGC 4608, NGC 5701, and NGC 5850 have evolved bars, the opposite is true for NGC 4394, NGC 4579, and NGC 5383, with recently formed bars. In agreement with the picture suggested by these theoretical models, the evolved bars are on average 2.1 kpc longer: The average L_B for evolved bars is 7.5 ± 1.2 kpc, and that for young bars is 5.4 ± 1.6 kpc. The average value of L_B for the whole sample is 5.0 ± 0.7 kpc. Similar results are obtained if one uses the length of the bar normalized by D_{25}.

It should be stressed that our sample is statistically small. The difference between L_B for young and old bars is reliable only at the 1 σ confidence level, and thus it is necessary to obtain bar age estimates for a larger galaxy sample. On the other hand, the length of the bar does not depend only on its age and the disk size. Athanassoula (2003) shows that bar strength depends on a series of factors, notably the ability of the disk and halo to exchange angular momentum via orbital resonances. This may partially explain the spread in our age $\times L_B$ relation.

4.3. *Bar Profiles*

It is interesting to ask whether young and old bars also have different luminosity profiles along their major and minor axes. In Figure 6 we plot these profiles separately for young and evolved bars and see no difference. All galaxies show luminosity profiles along their bar major axis with conspicuous plateaus, while their bar minor axis profiles are closer to exponential. As shown by Elmegreen & Elmegreen (1985), this is characteristic of bars in galaxies with morphological types earlier than Sbc.

5. DISCUSSION

The relation between bar color and age must be treated with care and at least two caveats kept in mind. First, we showed that young bars look bluer than old ones, but since young bars seem to be found mostly in late-type galaxies it must be checked whether this difference in bar color is not a result of the difference in the color of the galaxies as a whole, as late-type galaxies have generally integrated colors bluer than early-type galaxies (Roberts & Haynes 1994), with a large spread nevertheless. Second, it is not clear how the color of a bar would change when it captures stars from the disk as it evolves. In principle, one may argue that the capture of stars from the disk would tend to prevent it from getting redder and thus dilute the relation between bar age and color.

Table 5 shows a summary of the average properties of the bars in our sample concerning the galaxies' morphological types and the prominence of the bar according to the RC3. As expected, weak bars (in SAB galaxies) are shorter than the strong ones (SB). They are also bluer on average, as are bars in later type galaxies. It appears, however, that it could not be the case only that bluer bars reside in bluer galaxies and vice versa. That would represent a bias toward pointing to younger bars in later type galaxies. To assess this issue we can take from LEDA integrated $B - V$ colors (corrected to face-on) of those galaxies for which we have bar age estimates and compare them. The mean global $B - V$ color of galaxies with old bars is 0.81 ± 0.05, whereas that of galaxies with young bars is 0.72 ± 0.06. Although there seems to be a difference (0.09 mag), it appears too small to explain the difference we found in the $B - V$ color of young and old bars, which is of 0.40 mag. Hence, the result on the bluer bars of SAB galaxies may be genuine and point to a very interesting conclusion. SAB bars may be the ones that are passing through processes of formation, or, alternatively, dissolution. However, their bluer colors suggest they are forming, and thus young, bars. Furthermore, either the processes of bar dissolution are significantly faster than those of bar formation, or bar dissolution is much less frequent than bar formation, since, otherwise, those dissolving bars, with their old and red stellar population, would dilute this difference in color.

One may also argue that the capture of disk stars by the bar does not turn it bluer—first, because the bar originates from the same stellar population that makes up the original disk, and, second, because after the star-forming bursts along the recently formed bar fade new stars will mostly appear within the disk only outside of the bar region. Gas in the disk is collected by the bar and funneled away from the bar region. It is evident that further theoretical and observational studies on the evolution of bars and its effects on the overall star formation in galaxies are necessary to clarify these issues, as is a large sample of galaxies with good estimates for bar ages, colors, and lengths.

In Paper I (see also Gadotti & de Souza 2004) we find that galaxies with active galactic nuclei (AGNs) tend to have young

TABLE 5
AVERAGE PROPERTIES OF BARS

Type	L_B (kpc)	$(B - I)_B$
0–0/a	4.4 (0.9)	2.08 (0.14)
a–ab	4.6 (1.1)	1.67 (0.09)
b–bc	6.2 (1.5)	1.55 (0.20)
SAB	3.4 (0.4)	1.55 (0.14)
SB	5.9 (0.9)	1.90 (0.14)

NOTE.—Standard error in parentheses.

bars, while galaxies with old bars do not generally have AGNs. This leads us to conclude that the fueling of AGNs by bars occurs in short timescales, i.e., of the order of 1 Gyr or less. Here we also find results that corroborate this conclusion if we assume the $B - I$ color of the bars as a good index of the bars' ages. In fact, the $B - I$ color of the bars in galaxies with AGNs in our sample is 1.63 ± 0.11, whereas this goes to 2.03 ± 0.19 in galaxies without AGNs. Hence, it appears that the building of a gas reservoir for AGNs by a bar occurs in the bar first evolutionary stages. As galaxies with AGNs are generally of early type, it is not likely that this difference in bar color results from the difference in color of the galaxies as a whole, as the trend would thus be opposite.

Laurikainen et al. (2004 and references therein) show that the bars in galaxies with AGNs, while being massive, may have a weaker impact on the overall galaxy evolution when compared to galaxies without AGNs. Considering that the amount of fuel necessary to ignite an AGN episode is *very* small (see, e.g., Jogee 2004) this result is not as surprising as it may appear. In this context it is worth stressing here that when comparing different bars the fact that one is longer does not necessarily mean that it produces greater changes in the galaxy mass distribution. As shown by Laurikainen et al. (2004), if there is a prominent bulge, its effects on the force distribution along the galaxy will dilute those effects caused by the bar. However, when one says that a bar grows longer, as in Athanassoula's models, it is obvious that it also grows stronger, as it gets more massive, and possibly more eccentric, unless the bulge also grows more important accordingly.

Another relevant question concerns the possibility of recurrent bars. In this regard, it is interesting that from the spectroscopy results in Paper I we find among evolved bars 7 of 8 galaxies with morphological types S0–Sa, and only 1 of 8 galaxies of type Sb. On the other hand, from the 5 galaxies with young bars, 2 are S0–Sa galaxies, and 3 are Sb galaxies. This is interesting considering the suggestion by Friedli & Benz (1995) that bars are young in late-type galaxies and more evolved in early-type galaxies. This is also consistent with our conclusion that SAB galaxies have young bars, as we find in Gadotti & de Souza (2004) that SAB galaxies occur preferentially in the Sc bin of the morphological classification scheme. Unless bars are recurrent and contribute significantly to bulge building only in late-type galaxies, these findings challenge bar recurrent scenarios such as the one by Bournaud & Combes (2002). If bars are recurrent and contribute to the formation of bulges along the Hubble sequence, we should not observe a higher fraction of young bars in one narrow range of morphological types. In the Bournaud & Combes (2002) scenario bars die and are reborn with ever shorter lengths and faster pattern rotation velocities, Ω_B. If bars are not recurrent, however, and grow longer while aging, then we should expect Ω_B to fall in early-type galaxies. The results concerning this physical parameter are still very rare (especially in late-type galaxies) but initially point to lower values for Ω_B in early-type galaxies (Gerssen et al. 2003). Thus, it seems that the models of Bournaud & Combes (2002) are not consistent with the observations. In the recurrent models of Berentzen et al. (2004) bars reappear with a lower rotation velocity, but these results only apply for galaxies that lack gas and when bars result from tidal forces provoked by a close companion. Another argument against the Bournaud & Combes (2002) recurrent bar scenario, based directly on bar sizes, has recently been made by Erwin (2005).

The correlation found by Athanassoula & Martinet (1980), that more prominent bulges appear in galaxies with longer bars is also an argument that favors a scenario in which as bars age and grow longer they contribute secularly to bulge building. Furthermore, if this picture is correct, then we should not expect that bars are recurrent, since in this case we should observe young, short bars in galaxies with big bulges, which is not the case. Hence, if bar formation processes are similar in early- and late-type galaxies, it seems that either bars are recurrent only in galaxies with morphological types around Sc or they are generally not recurrent at all.

We thank Rob Kennicutt for his kind hospitality and for giving us access to the Steward Observatory telescopes. It is a pleasure to thank Lia Athanassoula for her comments on a first draft of this article. We are thankful to the anonymous referee for a careful reading of the manuscript and for many useful remarks. This work was financially supported by FAPESP grants 99/07492-7 and 00/06695-0. This research has made use of the NASA/IPAC Extragalactic Database (NED), which is operated by the Jet Propulsion Laboratory, California Institute of Technology, under contract with the National Aeronautics and Space Administration. This research has also made use of NASA's Astrophysics Data System and of the HyperLeda database (http://leda.univ-lyon1.fr/).

REFERENCES

Athanassoula, E. 2002, ApJ, 569, L83
———. 2003, MNRAS, 341, 1179
———. 2005, MNRAS, 358, 1477
Athanassoula, E., & Martinet, L. 1980, A&A, 87, L10
Athanassoula, E., & Misiriotis, A. 2002, MNRAS, 330, 35
Berentzen, I., Athanassoula, E., Heller, C. H., & Fricke, K. J. 2004, MNRAS, 347, 220
Bournaud, F., & Combes, F. 2002, A&A, 392, 83
de Jong, R. S. 1996, A&A, 313, 377
de Vaucouleurs, G., de Vaucouleurs, A., Corwin, H. G., Buta, R. J., Paturel, G., & Fouque, P. 1991, Third Reference Catalog of Bright Galaxies (New York: Springer) (RC3)
Eggen, O. J., Lynden-Bell, D., & Sandage, A. R. 1962, ApJ, 136, 748
Elias, J. H., Frogel, J. A., Matthews, K., & Neugebauer, G. 1982, AJ, 87, 1029
Elmegreen, B. G., & Elmegreen, D. M. 1985, ApJ, 288, 438
Elmegreen, B. G., Elmegreen, D. M., & Hirst, A. C. 2004, ApJ, 612, 191
Elmegreen, D. M. 1998, Galaxies and Galactic Structure (Englewood Cliffs: Prentice Hall)
Erwin, P. 2004, A&A, 415, 941
———. 2005, MNRAS, in press (astro-ph/0508590)
Erwin, P., & Sparke, L. S. 2002, AJ, 124, 65
———. 2003, ApJS, 146, 299
Friedli, D., & Benz, W. 1995, A&A, 301, 649
Fukugita, M., Shimasaku, K., & Ichikawa, T. 1995, PASP, 107, 945
Gadotti, D. A., & de Souza, R. E. 2003a, ApJ, 583, L75
———. 2003b, Ap&SS, 284, 527
———. 2004, in IAU Symp. 222, The Interplay among Black Holes, Stars and ISM in Galactic Nuclei, ed. Th. Storchi Bergmann, L. C. Ho, & H. R. Schmitt (Dordrecht: Kluwer), 423
———. 2005, ApJ, 629, 797 (Paper I)
Gadotti, D. A., & dos Anjos, S. 2001, AJ, 122, 1298
Gerssen, J., Kuijken, K., & Merrifield, M. R. 2003, MNRAS, 345, 261
Giovanelli, R., Haynes, M. P., Salzer, J. J., Wegner, G., da Costa, L. N., & Freudling, W. 1994, AJ, 107, 2036
Jogee, S. 2004, LNP Volume on AGN Physics on All Scales, Chapter 6, in press (astro-ph/0408383)
Jogee, S., et al. 2004, ApJ, 615, L105
Jungwiert, B., Combes, F., & Axon, D. J. 1997, A&AS, 125, 479
Kitchin, C. R. 1998, Astrophysical Techniques (Bristol: Inst. Physics)
Kormendy, J., & Kennicutt, R. C. 2004, ARA&A, 42, 603
Laine, S., Shlosman, I., Knapen, J. H., & Peletier, R. F. 2002, ApJ, 567, 97
Landolt, A. U. 1983, AJ, 88, 439
Laurikainen, E., Salo, H., & Buta, R. 2004, ApJ, 607, 103
Maraston, C. 1998, MNRAS, 300, 872

Martin, P. 1995, AJ, 109, 2428
Martin, P., & Friedli, D. 1997, A&A, 326, 449
Martin, P., & Roy, J.-R. 1995, ApJ, 445, 161
Persson, S. E., Murphy, D. C., Krzeminski, W., Roth, M., & Rieke, M. J. 1998, AJ, 116, 2475
Phillips, A. C. 1993, Ph.D. thesis, Univ. Washington
———. 1996, in ASP Conf. Ser. 91, Barred Galaxies, ed. R. Buta, D. A. Crocker, & B. G. Elmegreen (San Francisco: ASP), 44
Roberts, M. S., & Haynes, M. P. 1994, ARA&A, 32, 115
Schlegel, D. J., Finkbeiner, D. P., & Davis, M. 1998, ApJ, 500, 525
Searle, L., & Zinn, R. 1978, ApJ, 225, 357
Shen, J., & Sellwood, J. A. 2004, ApJ, 604, 614
Spitzer, L., & Schwarzschild, M. 1951, ApJ, 114, 385
———. 1953, ApJ, 118, 106
Tinsley, B. M., & Gunn, J. E. 1976, ApJ, 203, 52
Wozniak, H., Friedli, D., Martinet, L., Martin, P., & Bratschi, P. 1995, A&AS, 111, 115